



HAL
open science

Characterization of liposome-containing SPIONs conjugated with anti-CD20 developed as a novel theranostic agent for central nervous system lymphoma

S. Saesoo, S. Sathornsumetee, P. Anekwiang, C. Treetidnipa, P. Thuwajit, S. Bunthot, W. Maneepprakorn, Lionel Maurizi, H. Hofmann, Ruktanonchai Uracha Rungsardthong, et al.

► To cite this version:

S. Saesoo, S. Sathornsumetee, P. Anekwiang, C. Treetidnipa, P. Thuwajit, et al.. Characterization of liposome-containing SPIONs conjugated with anti-CD20 developed as a novel theranostic agent for central nervous system lymphoma. *Colloids and Surfaces B: Biointerfaces*, 2018, 161, pp.497-507. 10.1016/j.colsurfb.2017.11.003 . hal-02163452

HAL Id: hal-02163452

<https://hal.science/hal-02163452>

Submitted on 14 Mar 2021

HAL is a multi-disciplinary open access archive for the deposit and dissemination of scientific research documents, whether they are published or not. The documents may come from teaching and research institutions in France or abroad, or from public or private research centers.

L'archive ouverte pluridisciplinaire **HAL**, est destinée au dépôt et à la diffusion de documents scientifiques de niveau recherche, publiés ou non, émanant des établissements d'enseignement et de recherche français ou étrangers, des laboratoires publics ou privés.

1 **Characterization of liposome-containing SPIONs conjugated with anti-CD20 developed**
2 **as a novel theranostic agent for central nervous system lymphoma**

3

4 **S. Saesoo S⁽¹⁾, S. Sathornsumetee^(2,5), P. Anekwiang⁽²⁾, C. Treetidnipa⁽²⁾,**
5 **P. Thuwajit^(2,4), S. Bunthot⁽¹⁾, W. Maneepakorn⁽¹⁾, L. Maurizi⁽⁶⁾, H. Hofmann⁽⁷⁾,**
6 **Ruktanonchai Uracha Rungsardthong⁽¹⁾, N. Saengkrit⁽¹⁾**

7

8 **(1) National Nanotechnology Center (NANOTEC), National Science and Technology**
9 **Development Agency (NSTDA), Pathumthani 12120, Thailand**

10 **(2) NANOTEC-Mahidol University Center of Excellence in Nanotechnology for Cancer**
11 **Diagnosis and Treatment and Departments of (3) Radiology, (4) Immunology and (5)**
12 **Medicine, Faculty of Medicine Siriraj Hospital, Mahidol University 2 Wanglang Road,**
13 **Bangkoknoi, Bangkok 10700, Thailand**

14 **(6) Laboratoire Interdisciplinaire Carnot de Bourgogne, UMR 6303 CNRS—Université**
15 **Bourgogne Franche-Comté, BP 47870, F-21078 Dijon cedex, France**

16 **(7) Powder Technology Laboratory, Ecole Polytechnique Fédérale de Lausanne (EPFL),**
17 **1015 Lausanne, Switzerland.**

18

19 **1. Introduction**

20 Despite advances in the understanding of genetic and molecular abnormalities relating
21 to cancer, and in development of new therapies, the prognosis of patients with primary central
22 nervous system lymphoma (PCNSL) remains poor when compared to other lymphoma types
23 (median survival 3-5 years) [1]. For immunocompromised patients, such as those with AIDS
24 or in cases of organ transplantation, median survival times are often markedly reduced
25 (typically less than 1 year) [2]. Due to this, and the rising incidence of PCNSL over the past
26 decades there is a need to develop new diagnostic and therapeutic strategies which are
27 applicable to these patients, including the wider population [3].

28 PCNSL accounts for 3-5% of primary brain tumors in adults, and occurs with an
29 incidence of 5 per 1,000,000 people in developed countries [1]. Most (> 95%) PCNSL cases
30 are of the diffuse large B-cell type. Genetic abnormalities in PCNSL cells are distinct from
31 those occurring in other lymphomas; this factor may relate to observed differences in prognosis
32 and treatment response [4]. Non-invasive imaging studies such as magnetic resonance imaging
33 (MRI) and positron-emission tomography (PET) scans can support an initial diagnosis of
34 PCNSL, however confirmation usually requires a stereotactic biopsy. Alternatively, cytology
35 of cerebrospinal fluid, or ocular vitreous, may confirm diagnosis in 20-30% of patients.
36 Diagnosis of AIDS-associated PCNSL represents an important challenge in clinical practice.
37 Radiographic findings of PCNSL in immunocompromised patients are often indistinguishable
38 from infections, particularly toxoplasmosis. In these cases, biopsies are often deferred until the
39 empiric treatment for toxoplasmosis fails, causing delays in diagnosis. Therefore, non-invasive
40 diagnostic approaches, such as neuroimaging probes, for PCNSL in AIDS patients may hasten
41 diagnosis allowing early treatment. High-dose methotrexate (HD-MTX)-based chemotherapy
42 regimens are the standard treatment for PCNSL [5], and these combined with other
43 chemotherapies (cytarabine, procarbazine, vincristine, or ifosfamide) have been shown to
44 provide superior results in some cases, although the higher toxicity is a serious issue. RTX, a
45 monoclonal antibody against CD20, has demonstrated promising activity as a single agent in
46 PCNSL [6], despite the inherent limitation of such a large molecule in traversing the blood-
47 brain barrier [7, 8]. Employing nanoparticles as a carrier for RTX may help overcome this
48 challenge, and result in increased efficacy in PCNSL treatment.

49 The blood-brain barrier represents a major obstacle for drug delivery to the CNS [9,
50 10]. The use of a small lipophilic carrier, such as a nanoparticle system, may overcome this
51 problem, with nanoparticles allowing for improved drug delivery metrics as well as diagnostic
52 and monitoring capabilities. This emerging molecular platform, “theranostics” [11], employs
53 nanoparticle systems based on liposomes [12], micelles [13], and dendrimers [14] to protect
54 drugs and deliver them to targets in a controlled manner. In addition, they can be decorated
55 with “molecular antennae” such as antibodies or aptamers on their surface to allow target
56 specificity. Imaging probes are an important group of theranostic particles: these can be
57 detected *in vivo* through various imaging modalities [15]. Superparamagnetic iron oxide
58 nanoparticles (SPIONs) and radioisotopically labelled nanoparticles are common imaging
59 probes detectable by magnetic resonance imaging and positron emission tomography,
60 respectively. Among the various nanoparticle classes available, liposomes have shown real

61 promise in the treatment of brain disorders [16-18], having been shown to enhance the delivery
62 of neuroprotective agents to the peri-infarct area in experimental ischemic stroke models [17,
63 18]. In this study, we fabricated nanoparticles consisting of liposome containing SPIONs
64 decorated with RTX, and subsequently evaluated their imaging and targeting abilities,
65 including therapeutic potency, in a BBB model of PCNSL.

66 **2. Materials and methods**

67 **2.1 Materials**

68 Soybean lecithin (Soya Phosphatidylcholin; PC) was purchased from Degussa
69 (Hamburg, Germany). 1,2-Distearoyl-sn-glycero-3-phosphoethanolamine-N-
70 [amino(polyethylene glycol 2000)] (DSPEG-PE), and 1,2-dioleoyl-sn-glycero-3-
71 phosphoethanolamine-N-[4-(p-maleimidophenyl)butyramide] (MPB-PE, linker) were
72 purchased from Avanti Polar Lipids, Inc (Alabama, USA). Cholesterol was also obtained from
73 Avanti Polar Lipids, Inc (Alabama, USA). Polysorbate 80 (Tween 80) was obtained from
74 Sigma-Aldrich (Saint Louis, MO, USA). Phosphate buffered saline (pH 7.4) (PBS; containing
75 137 mM NaCl, 2.7 mM KCl, 10 mM Na₂HPO₄; 2 mM KH₂PO₄), and Triton X-100 were
76 obtained from Merck (Merck Millipore, Darmstadt, Germany). Anti-CD20 (RTX) was
77 purchased from Roche (Basel, Switzerland). Roswell Park Memorial Institute media (RPMI
78 1640) was from GIBCO Invitrogen (New York, USA). Fetal bovine serum (FBS) was obtained
79 from Biochrom AG (Berlin, Germany). Trypsin-EDTA, L-glutamine, penicillin G sodium,
80 streptomycin sulfate, and amphotericin B were obtained from Invitrogen Corp. (New York,
81 USA). MTT [3-(4,5-Dimethylthiazol-2-yl)-2,5-diphenyltetrazolium bromide] was purchased
82 from GIBCO Invitrogen (NY, USA). Dimethylsulfoxide (DMSO) was procured from Sigma-
83 Aldrich, Inc, (Dorset, UK). The Annexin V-FITC Apoptosis Detection Kit was obtained from
84 NeXins Research BV (Rotterdam, the Netherlands). Distilled water was generated using an
85 ELGA system (PureLab Ultra, Illinois, USA). Z138C and Granta519 lymphoma cell lines were
86 graciously provided by Dr. Siwanon Jirawatnotai (Bangkok, Thailand). SPIONs-PVA
87 nanoparticles were kindly provided by Prof. Heinrich Hofmann and Dr. Lionel Maurizi (EPFL,
88 Switzerland). These particles were synthesized from maghemite (γ -Fe₂O₃), affording SPIONs
89 having a diameter less than 20 nm. All SPIONs were coated with PVA (Polyvinyl alcohol) for
90 stabilization [19] and called SPION-PVA.

91 **2.2 Lymphoma cell cultivation**

92 Granta and Z138C cell lines were cultured in RPMI 1640 medium. The medium was
93 supplemented with 10% FBS containing 0.1 mM non-essential amino acids (100 µg/ml L-
94 glutamine, 100 µg/ml streptomycin and 100 U/ml penicillin). Cells were grown and propagated
95 in 75 ml T-flasks, and incubated at 37°C in a humidified atmosphere containing 5% CO₂. The
96 medium was changed every other day.

97 **2.3 Preparation of liposomes and conjugation of RTX**

98 A series of liposome nanoparticles were prepared by conventional thin film hydration,
99 which involved the mixing of PC, DSPEG-PE, Tween 80 and MPB-PE (linker) in various
100 proportions, as indicated in Table 1. Each mixture was then dissolved in chloroform-diethyl
101 ether (3:1 v/v, 10 ml), and upon solvent removal by rotary evaporation at 25°C under 50-100
102 kg/cm² nitrogen flow thin lipid films were obtained. After drying, lipid films were rehydrated
103 with 0.2 mg_{Fe}/ml of SPION-PVA dissolved in PBS (pH 7.4), and re-suspended with shaking at
104 room temperature. Particle sizes of all liposome samples were reduced using a discontinuous
105 extruder (Liposo-Fast™-10, Avestin Inc, Ottawa, Canada) operating at 200 bar pressure over
106 15-20 cycles, through a 200 nm pore size polypropylene membrane (Millipore GmbH,
107 Eschborn, Germany). The SPIONs-PVA loaded liposomes were purified by centrifugation
108 (TomyMX-301, Tokyo, Japan) at 10,000 rpm for 30 min, prior to collection. The obtained
109 pellets were re-suspended in PBS (pH 7.4) buffer for measuring of SPION entrapment.
110 Additionally, in order to obtain an optimized formulation for BBB delivery, the following
111 liposome series were initially prepared: liposome (Lip), Lip/PEG, Lip/Tween80,
112 Lip/PEG/Tween80, Lip/PEG/Tween80 and Lip/PEG/Tween80/RTX.

113 Immobilization of RTX was performed via chemical conjugation. Thiolated RTX was
114 firstly prepared by mixing RTX with 2-iminothiolane at 25°C for 30 min. The conjugation of
115 RTX and liposomes was achieved via the coupling of thiolated RTX and MPB-PE onto the
116 liposome surface. This required gradual addition of MPB-PE-liposomes into the freshly
117 prepared thiolated RTX, followed by incubation of the solution at 4°C overnight under nitrogen
118 atmosphere, with continuous stirring. The resultant RTX conjugated liposomes were purified
119 by ultracentrifugal sedimentation at 60,000 rpm for 90 min, and the obtained pellets were re-
120 suspended and washed twice with PBS buffer (pH 7.4).

121 **2.4 Morphology and physicochemical characterization of liposomes**

122 The morphology of liposomes was investigated using transmission electron microscopy
123 (TEM). Samples were prepared by placing 5 μ l of liposome solution onto a 200-mesh carbon
124 copper grid (EMS Equipment, Berks, UK). After 10 min, the droplet was removed from the
125 edge of the grid using filter paper. Samples were dried by standing at room temperature prior
126 to imaging: TEM (model JEM 2010; JEOL, Peabody, MA) accelerating voltage 120 KV, 50 K
127 magnification.

128 Hydrodynamic diameter, polydispersity index (PDI) and zeta potential of liposomes
129 were determined by dynamic light scattering (DLS) (NanoZS4700 nanoseries, Malvern
130 Instruments, Malvern, UK). All samples were diluted with 1 ml of filtered distilled water prior
131 to measurements being taken to eliminate viscosity effects caused by the ingredients.
132 Hydrodynamic diameter (based on volume measurement), PDI and zeta potential were
133 obtained from the average of three measurements at 25°C. The refractive indices of liposomes
134 and water were set at 1.42 and 1.33, respectively.

135 **2.5 Determination of SPIONs-PVA encapsulation**

136 The encapsulation of SPIONs-PVA within liposomes was quantified using the Prussian
137 Blue assay, where samples were diluted for preparation of a calibration curve (at least 3 serial
138 dilutions required). Particle iron concentrations ($[\text{Fe}]$ in mg Fe mL^{-1}) were measured through a
139 colorimetric assay. SPIONs-PVA were first digested by incubation overnight with an equal
140 volume of 6M HCl. Then, 25 μ l of digested particles was mixed with 50 μ l of 5% w/v
141 $\text{K}_4\text{Fe}(\text{CN})_6$ in water (freshly prepared and covered with aluminium foil). The sample was
142 then shaken continuously for 15 min, followed by measurement of the iron content, which
143 measured from the reaction between $\text{K}_4[\text{Fe}(\text{CN})_6]$ and Fe^{3+} to give an intense blue product
144 (Prussian blue, $\text{Fe}_4[\text{Fe}(\text{CN})_6]_3$) whose optical density was measured at 690 nm using a
145 microplate spectrophotometer (SpectraMAX2, Molecular Devices GmbH, CA, USA). The
146 encapsulation efficiency was calculated using the equation below.

$$147 \quad \% EE = \frac{\textit{Total amount of determined SPION}}{\textit{Initial amount of SPION loading}} \times 100$$

148 **2.6 MTT assay**

149 To evaluate the toxicity of SPIONs-PVA loaded liposomes, cells were plated in 96-
150 well plates, each containing 90 μ l of RPMI with 10% fetal bovine serum at a density of 8,000

151 cells/well. When the cultures had reached confluency (typically 24 h after plating) they were
 152 exposed to SPIONs-PVA loaded liposomes at SPIONs-PVA concentrations of 0.0005, 0.001,
 153 0.0025, 0.005, 0.01 or 0.02 mg_{Fe}/ml. The treated cells were then incubated for 24 h at 37°C in
 154 a CO₂ atmosphere. After washing twice with PBS (pH 7.4), 25 µl of MTT solution was added
 155 into each well, followed by further incubation (4 h). The medium was then removed and
 156 replaced with 100 µl of dimethylsulfoxide, followed by further incubation for 30 min at 37°C.
 157 Following this, the absorbance of the colored solution was measured at 550 nm using a
 158 microplate reader (SpectroMAX, California, US), and the percentage cell viability was
 159 calculated using equation and compared with that of the control.

$$\% \text{ Cell survival} = \frac{(Ab_{550} \text{ sample} - Ab_{550} \text{ control})}{Ab_{550} \text{ control}} \times 100$$

160

161 where Ab_{550} = absorbance value at 550 nm

162 2.7 Stability of liposomes

163 Liposome samples were stored in PBS (pH 7.4) buffer at 4°C, and 25°C for prolonged
 164 periods to gauge their stability. Samples were taken periodically at intervals of 1, 3 and 4
 165 months and liposome stability monitored using particle diameter, polydispersity index (PDI)
 166 and zeta potential measurements. Each measurement was performed in triplicate, and expressed
 167 as an average value.

168 2.8 Magnetization analysis by VSM

169 The magnetic properties of SPIONs, SPIONs-PVA and SPIONs-PVA loaded into Lip,
 170 Lip/PEG, Lip/Tween80 and Lip/PEG/Tween80/linker liposomes were assessed using vibrating
 171 sample magnetometry (VSM, LakeShore Model 7404, USA). For this, all samples were freeze-
 172 dried in liquid nitrogen and lyophilized under vacuum. The magnetic field was applied at 10
 173 kOe in all measurements.

174 2.9 Cellular uptake of liposomes

175 Internalization of liposomes was monitored by confocal laser scanning microscopy
 176 (CLSM), and flow cytometry. To monitor liposome uptake, Lip/PEG-PE and Lip/PEG-
 177 PE/RTX were labeled with Dil dye tracer (Invitrogen, Paisley, UK) at a ratio of 1:1000 v/v.
 178 Granta and Z138C cells (1×10^6 cells) were seeded onto sterilized glass coverslips and allowed

179 to adhere overnight in a 6-well plate. At transfection, Dil labeled liposomes were added to the
180 cells at a concentration of 0.4 mg/ml, which corresponds to the IC₂₀ value indicating 80% cell
181 viability. For CLSM, cell and liposome particles were incubated together for 2 h at 37°C under
182 an atmosphere of 5% CO₂. Cells were then washed twice with PBS (pH 7.4), fixed with 4%
183 w/v paraformaldehyde for 10 min, and then twice washed again with PBS (pH 7.4). For cellular
184 DNA staining, Hoechst dye (Molecular Probes, OR, USA) was diluted in PBS (pH 7.4) buffer
185 at a ratio of 1:1500 v/v, then incubated with the cells for 10 min. Cells were washed twice with
186 PBS pH 7.4 after staining then observed under confocal microscope. Images were acquired
187 using a laser scanning confocal microscope (Nikon, ECLIPSE Ti-Cls4 Laser Unit, Japan),
188 using the 60 objective lens. SPIONs-PVA detection was achieved by reflecting laser scanning,
189 with laser excitation at 488 nm.

190 Flow cytometry was employed to quantify cell internalization of liposomes. Cells were
191 cultivated in 6-well plates until growth levels reached 80% confluence. After washing with
192 PBS, cells were incubated with Dil-labeled SPION-PVA loaded liposomes (phosphatidyl
193 choline: Dil 1:500 w/w) at a concentration corresponding to the IC₂₀ value. Cellular
194 internalization of liposomes was quantified with time: after incubation for 30 min, 1, 2 and 4 h
195 unbound liposomes were removed by washing three times with PBS. At each time point,
196 internalization signals were analyzed using a flow cytometer (BD FACS Calibur™, BD
197 biosciences, CA, USA) at excitation and emission wavelengths of 488 and 600 nm,
198 respectively.

199 **2.10 Apoptosis assay**

200 Cells treated with liposomes were double stained with AnnexinV-FITC (AV-FITC) and
201 propidium iodide (PI) to detect apoptotic, and necrotic cells. AV-FITC/PI co-labeling was
202 performed according to the standard protocol as recommended by the manufacturer (BD
203 Pharmingen™, BD Biosciences, San Jose, CA, USA). Cells were seeded in a 6-well plate at a
204 density of 1×10^6 cells/well, and were allowed to attach for 24 h. After medium refreshment,
205 cells were exposed to either RTX, Lip, Lip/PEG-PE/SPIONs-PVA, Lip/PEG-
206 PE/Tween80/SPIONs-PVA or Lip/PEG-PE/Tween80/SPIONs-PVA/RTX at a concentration
207 corresponding to the IC₂₀ for 24 h at 37°C. Cells were then detached using trypsin-EDTA
208 solution, re-suspended in fresh medium, and centrifuged at 1,000 rpm for 5 min. The obtained
209 pellets were re-suspended in PBS (pH 7.4), centrifuged for a further 5 min (1,000 rpm), and
210 then collected and re-suspended in AnnexinV binding buffer. All samples were stained with 5

211 μl of AV-FITC and 10 μl of PI, and then incubated for 15 min in the dark at 25°C. After
212 addition of 250 μl of AnnexinV binding buffer to each, cells were analyzed using flow
213 cytometry (BDFACS CaliburTM, BD biosciences, San Jose CA, USA). The flow cytometer was
214 equipped with filters capable of detecting PI at excitation/emission wavelengths of 520/570
215 nm, while FITC was detectable at excitation/emission wavelengths of 485/535 nm. Results are
216 presented in a dot plot of AV-FITC versus PI with quadrant gating. The percentage apoptosis
217 in cells was determined using the FACSDiva software package.

218 **2.11 *In vitro* model BBB of PCNSL for permeability and therapeutic testing**

219 Permeability of the BBB can be gauged by measuring the transendothelial electrical
220 resistance (TEER), which affords a direct relation to its structural integrity. An *in vitro* co-
221 culture model of BBB was set up according to protocol of Imamura et al. [20]. For this, bEnd3
222 cells were seeded onto 0.4 μm pore size polyester membrane inserts (density of 20,000
223 cells/insert) contained in a 12-well plate transwell tray (Corning, NY, USA). The cells were
224 allowed to grow on the membrane for 8 days, with the DMEM medium being changed every 2
225 days. With this system, the drug targeting, and therapeutic effect, of RTX and liposomes on B
226 cell lymphoma cells was evaluated: for this, Granta cells were seeded at the bottom of the
227 culture dish and were allowed to grow for 4 days. After this time the TEER values were
228 monitored until they reached 140-150 $\Omega\cdot\text{cm}^2$ (approximately 7-10 days), after which the model
229 was ready for use in testing. Testing involved loading either free RTX,
230 Lip/PEG/Tween80/SPIONs-PVA or Lip/PEG/Tween80/SPIONs-PVA/RTX into separate
231 apical compartments of the co-culture model, with final concentrations of RTX (17.5 $\mu\text{g}/\text{ml}$)
232 coinciding with that of the IC_{50} of free RTX against Granta cells.

233 Determination of RTX concentrations in the membrane model was undertaken at set
234 time points (1, 2, 3, 5, 7 and 24 h) using the PK ELISA Kit (MyBioSource, CA, USA), with
235 harvesting of Granta cells at these times allowing evaluation of therapeutic effects. During the
236 24 h period, the TEER value was also monitored using a Millicell ERS-2 Voltohmmeter
237 (Millipore, MA, USA) for analysis of the permeability efficiency.

238 **3. Results and discussion**

239 **3.1. Morphology and physicochemical characterization of liposomes and encapsulation** 240 **efficiency**

241 TEM was employed to observe the morphologies of SPIONs-PVA, bare liposomes and
242 SPIONs-PVA loaded liposomes. While all samples were dehydrated for imaging, the
243 nanoparticles could be observed as having discrete spherical shapes (Fig. 1). SPIONs-PVA
244 showed a narrow size distribution (< 20 nm) (Fig. 1a). Liposomes fabricated in the absence of
245 added nanoparticles are spherical in shape but show slight deformations (Fig. 1b and c), while
246 SPIONs-PVA loaded liposomes exhibit a more pristine spherical profile as a result of tight
247 cargo packing resulting in size reduction, and enhanced stability, under TEM voltage exposure
248 (Fig. 1d and e).

249 Average hydrodynamic diameters, PDI and zeta potentials for bare, and SPIONs-PVA
250 loaded liposomes were obtained using DLS, with data summarized in Table 1. In the absence
251 of cargo, the diameters of Lip (control), Lip/PEG, Lip/Tween80, Lip/PEG/Tween80 and
252 Lip/PEG/Tween80/RTX liposomes were 141.9 ± 1.0 nm, 169.9 ± 11.3 nm, 161.0 ± 12.6 nm,
253 157.2 ± 9.1 nm and 182.0 ± 6.3 nm, respectively. Consistent with TEM results, loading of
254 SPIONs-PVA induces liposome contraction, an effect perhaps related to strong hydrophilic
255 interactions between liposome phospholipids and the PVA coating of SPIONs, which would
256 underpin their stability under TEM conditions [21]. The PDI index of all liposomes, being in
257 the range of 0.1 to 0.3, is indicative of homogeneity and narrow size distribution, which is again
258 consistent with findings from TEM. Loading of SPIONs-PVA results in liposome surface
259 charges becoming more negative, with these having zeta potentials ranging from -2.3 to -9.0
260 mV, depending on liposome composition. This result probably relates to the interaction of the
261 SPIONs-PVA surface with PC in the liposome membrane. Surface modification of liposomes
262 via RTX conjugation also affected their physicochemical properties: the zeta potential of bare
263 liposome (Lip) was -0.1 mV, whereas that of Lip/PEG/Tween80/RTX became more negative
264 (-7.2 mv) (Table 1).

265 SPIONs-PVA liposome loadings were quantified using the Prussian Blue assay as
266 described in section 2.5. From this data encapsulation efficiencies (%EE) for each liposome
267 formula were obtained (Table 1). A notable effect resulted from inclusion of Tween 80 into the
268 liposome structure: this resulted in remarkably higher entrapment (higher %EE) of SPIONs-
269 PVA relative to other liposome formulations. It is assumed that Tween80 incorporation into
270 the film helps to promote liposome stability, and prevents egress of SPIONs-PVA during
271 preparation [22].

272 **3.2. Liposome cytotoxicity**

273 The toxicity of SPIONs-loaded liposome formulas was analyzed using Z138c as a
274 lymphoma cell model, in order to evaluate their safety. All liposomes showed concentration-
275 dependent cytotoxicity, although no significant effects to cells were evident on exposure to
276 bare SPIONs-PVA (Fig. 2). Liposome solutions having SPIONs-PVA concentrations less than
277 0.0025 mg/ml were considered safe, as exposure to these resulted in greater than 80% cell
278 survival rates. Higher cytotoxicities were found for Tween80 fabricated liposomes; addition of
279 Tween 80 may enhance cellular uptake via ApoE ligand-mediated endocytosis [23]. However,
280 for these systems cell viabilities are still in the acceptable range although optimization of
281 liposome concentrations needs to be addressed to further their use in theranostic applications.

282 **3.3. Stability of liposomes**

283 In this study, we determined the stability of liposomes on storage at 4°C and 25°C.
284 Particle diameter, PDI and zeta potential of Lip, Lip/PEG/Tween20/SPIONs and
285 Lip/PEG/Tween20/SPIONs/RTX were measured periodically (1, 3 and 4 months) after storage
286 (Table 2). In regards to diameter and zeta potential of colloidal liposomes, for both
287 temperatures all formulations were stable for up to 3 months. Liposome stability could be
288 prolonged for a further month at 4°C, in contrast to results at 25°C which show dramatic
289 changes in zeta potential during the 4th month of storage. This would indicate aggregation of
290 liposome particles over time, as reflected by an increase in particle diameter. However,
291 diameter increases, and zeta potential changes are less marked in Tween80 supplemented
292 liposomes, the enhanced stability of these being consistent with previous work highlighting the
293 use of Tween80 as a non-ionic surfactant to improve liposome stability [22].

294 **3.4. Magnetic property analysis by vibrating scanning magnetometry (VSM)**

295 Vibrating scanning magnetometry (VSM) was performed to confirm the
296 superparamagnetic properties of SPIONs-loaded liposomes. Figure 3 highlights magnetization
297 curves, and saturation magnetization of SPIONs-PVA (0.5 mg/ml), and the series of liposomes:
298 Lip, Lip/PEG/SPION-PVA, Lip/PEG/Tween80/SPION-PVA, and Lip/PEG/Tween80/SPION-
299 PVA/RTX. The saturation magnetization values of naked SPIONs were also determined, as a
300 positive control. The hysteresis curves of SPIONs-loaded liposomes showed an absence of
301 remanence, and this, in conjunction with the magnetization on average being zero, indicates
302 that the SPIONs exhibit superparamagnetic behavior. Although the saturated magnetization
303 value of naked SPIONs was found to be 28.9 emu/g, coating with PVA results in a drastic
304 magnetization decrease (1.5 emu/g). This effect has been noted previously, for example in PVA

305 coated magnetite magnetic [24], and silica coated magnetic nanoparticles [25]. For SPIONs-
306 PVA loaded liposomes, the saturated magnetization values were in range of 0.2-0.5 emu/g (Fig.
307 3). This magnetization range corresponds to those of SPIONs obtained from maghemite (γ -
308 Fe_2O_3), the values of which are thought to be lower than those from magnetite (Fe_3O_4) [26].
309 These findings are a preliminary step in the characterization of these systems, however for
310 actual implementation as theranostics further optimization of the magnetization value is
311 necessary.

312 **3.5. Liposome cellular internalization and uptake**

313 Cellular uptake, and distribution of liposomes and SPIONs-PVA was monitored by
314 confocal microscopy. Cells were treated with Lip/PEG/Tween80/SPIONs-PVA and
315 Lip/PEG/Tween80/SPIONs-PVA/RTX, according to the protocol described in section 2.9. At
316 2 h post incubation, SPIONs-PVA were detectable within cells (as shown in green) by
317 reflecting laser scanning (excitation at 488 nm), while liposome nanoparticles appear red due
318 to the presence of Dil (Fig. 4). Z-stack imaging analysis confirmed internalization of the
319 particles within the liposomes (data not shown). Confocal imaging indicated that signal
320 intensities of Lip/PEG/Tween80/SPIONs-PVA/RTX were significantly higher than those of
321 Lip/PEG/Tween80/SPIONs-PVA, both in Z138c and Granta cell lines (Fig. 4a and 4b). These
322 results imply that conjugation of RTX promotes liposome internalization and provides
323 evidence supporting that binding of RTX occurs selectively on CD-20 presenting lymphoma
324 cells.

325 To confirm targeting of RTX conjugates with CD-20 lymphoma cells, we then
326 monitored the cellular uptake of liposomes quantitatively by flow cytometry.
327 Lip/PEG/Tween80/SPIONs-PVA and Lip/PEG/Tween80/SPIONs-PVA/RTX were incubated
328 with cultured cells, and uptake was monitored at times of 30 min, 1, 2, and 4 h. Histograms
329 obtained from flow cytometry analysis indicate that cellular internalization of liposomes is
330 time-dependent (Fig. 5). While liposome uptake takes place within 0.5 h-post incubation, the
331 signal intensities of Lip/PEG/Tween80/SPIONs-PVA and Lip/PEG/Tween80/SPIONs-
332 PVA/RTX were not equal, and were observed to change during the incubation period. In both
333 Granta and Z138c cell lines the signal intensity from Lip/PEG/Tween80/SPIONs-PVA/RTX
334 proved higher than that resulting from Lip/PEG/Tween80/SPIONs-PVA, which confirmed that
335 RTX functions as a specific antibody for selective binding to anti-CD20 receptors in lymphoma
336 cells.

337 **3.6. Apoptosis induction by RTX conjugated liposomes**

338 RTX is a mainstay in therapies for a broad variety of B-cell malignancies [27, 28]. It
339 induces direct apoptosis through binding to CD20 on the surface of lymphoma cells. In order
340 to verify targeting, and therapeutic effects of Lip/PEG/Tween80/SPIONs-PVA/RTX,
341 annexinV-FITC/PI staining was employed to monitor RTX-induced cell death. For this, Granta
342 and Z138c cell lines were incubated with free RTX (7.9 $\mu\text{g/ml}$), bare liposomes (Lip),
343 Lip/PEG/SPIONs-PVA, Lip/PEG/Tween80/SPIONs-PVA and Lip/PEG/Tween80/SPIONs-
344 PVA/RTX (at the IC_{20} concentration) for 24 h at 37°C. Cells were then removed to determine
345 the degree of apoptosis using flow cytometry. In Fig. 6a and 6b, the lower right quadrant shows
346 annexin positive cells (early apoptotic stage) and the upper right quadrant shows annexin and
347 PI positive cells (late stage apoptosis). Lip/PEG/Tween80/SPIONs-PVA/RTX induced
348 apoptosis by a significantly high degree in both Granta and Z138c cells (by 65.4% and 43.1%,
349 respectively), while free RTX resulted in lower levels of apoptosis induction (18.3% and 16.7%
350 in Granta and Z138c cells, respectively). These results not only suggest that RTX exerts
351 therapeutic effects, but also illustrates the effect of liposome conjugation on the efficacy of
352 apoptosis induction. The presence of RTX on the surface of liposomes allows for advantageous
353 binding with the target cells in addition to facilitating its cellular uptake, in line with its role as
354 a therapeutic agent. Notably, treatment of cells with RTX-free liposomes results in less than
355 10% apoptosis, suggesting that the carrier itself is relatively benign.

356 **3.7 Transport of RTX across the BBB model**

357 In order to demonstrate transportation of our formulated liposome across the BBB, an
358 *in vitro* BBB model was established according to a previous protocol [20]. During the
359 investigation (over 24 h), TEER values of the cell control were constantly maintained at 140-
360 150 $\Omega\cdot\text{cm}^2$. After model development, it was loaded with free RTX and
361 Lip/PEG/Tween80/SPIONs-PVA/RTX, and these samples were allowed to pass the cell
362 monolayer for a set time period. The extent of transported RTX was quantified by ELISA
363 measurements at set time points, up to 24 h post-loading. The results revealed that free RTX is
364 not readily transported through the BBB membrane, although liposomes act as a facile delivery
365 system promoting cross-barrier transport (Fig. 7). Tween 80 may play a crucial role in
366 fabrication of this delivery system: previous work has highlighted its binding with ApoE on
367 bEnd3 endothelial cells [23]. Concentrations of RTX detected across the membrane were time-
368 dependent and were consistent with TEER values, except for the period at 5 h post incubation

369 where the level of permeable RTX may have been affected by the charge on the bEnd3
370 endothelial membrane.

371 **3.8 Evaluation of drug targeting therapeutic effect**

372 As the ability of RTX to be transported across the BBB is a major factor dictating its
373 therapeutic effects, the capacity of RTX to target Granta cells was evaluated in the BBB model
374 by analysis of cellular viability. Free RTX and Lip/PEG/Tween80/SPIONs-PVA/RTX were
375 loaded onto the BBB model, at an RTX concentration corresponding to the IC₅₀ (17.5 µg/ml).
376 At 24 h post incubation, Granta cells located at the basal layer were collected to evaluate cell
377 viability, in comparison with the control. The results shown in Fig. 8 indicate that, during the
378 incubation period, no effects relating to free RTX were observed. In contrast, exposure to RTX-
379 conjugated liposomes resulted in noticeable toxic effects after 5 h, with the level of toxicity
380 being time-dependent. This result confirmed that effective delivery of RTX across the BBB
381 requires a delivery system, and accordingly modified liposomes may be considered as an
382 appropriate vehicle for promoting therapeutic effects.

383 **4. Conclusion**

384 Diagnosis of primary CNS lymphoma currently relies on pathology derived from a
385 brain biopsy, which carries significant risk. Non-invasive neuroimaging protocols that can
386 accurately distinguish lymphoma from other disorders are urgently needed, particularly in
387 immunocompromised patients. In this study, we developed a new diagnostic nanoparticle
388 platform for CNS lymphoma consisting of SPIONs loaded liposomes conjugated with anti-
389 CD20 (RTX). Liposomal RTX may also exhibit activity against CNS lymphoma, although
390 preclinical evaluations of its efficacy are still being investigated.

391 A previous study has evaluated ferumoxytol (Feraheme), an iron oxide nanoparticle, as
392 an MRI contrast agent for primary CNS lymphoma and CNS inflammatory disorders [29].
393 From the immunofluorescence and flow cytometric results herein which demonstrate higher
394 specificity of anti-CD20-liposome-SPIONs for detection of lymphoma cells over classically
395 used coated SPIONs, and the ability of anti-CD20-liposome-SPIONs, despite their large size,
396 to cross the blood-brain barrier into lymphoma xenografts, it is possible that conjugation of
397 anti-CD20 as a targeting moiety in the liposome-SPION complex will result in greater
398 specificity for lymphoma detection by MRI than is possible in other contrast agents (such as
399 gadolinium and ferumoxytol). Accordingly, anti-CD20-liposome-SPIONs may serve as a

400 promising theranostic MRI contrast agent for specific detection, and monitoring of CNS
401 lymphoma.

402

- 403 1. Behin, A., et al., *Primary brain tumours in adults*. The Lancet, 2003. **361**(9354): p. 323-331.
- 404 2. Subsai, K., et al., *Neurological complications in AIDS patients receiving HAART: a 2-year*
405 *retrospective study*. European journal of neurology, 2006. **13**(3): p. 233-239.
- 406 3. Olson, J.E., et al., *The continuing increase in the incidence of primary central nervous system*
407 *non-Hodgkin lymphoma*. Cancer, 2002. **95**(7): p. 1504-1510.
- 408 4. Tun, H.W., et al., *Pathway analysis of primary central nervous system lymphoma*. Blood,
409 2008. **111**(6): p. 3200-3210.
- 410 5. Batchelor, T. and J.S. Loeffler, *Primary CNS lymphoma*. Journal of Clinical Oncology, 2006.
411 **24**(8): p. 1281-1288.
- 412 6. Birnbaum, T., et al., *Successful long-term control of lymphomatous meningitis with*
413 *intraventricular rituximab*. Journal of Clinical Neuroscience, 2014. **21**(2): p. 356-358.
- 414 7. Gerstner, E.R., et al., *Long-term outcome in PCNSL patients treated with high-dose*
415 *methotrexate and deferred radiation*. Neurology, 2008. **70**(5): p. 401-402.
- 416 8. Batchelor, T., et al., *Rituximab monotherapy for patients with recurrent primary CNS*
417 *lymphoma*. Neurology, 2011. **76**(10): p. 929-930.
- 418 9. Bicker, J., et al., *Blood-brain barrier models and their relevance for a successful development*
419 *of CNS drug delivery systems: a review*. European Journal of Pharmaceutics and
420 Biopharmaceutics, 2014. **87**(3): p. 409-432.
- 421 10. Gribkoff, V.K. and L.K. Kaczmarek, *The Need for New Approaches in CNS Drug Discovery: Why*
422 *Drugs Have Failed, and What Can Be Done to Improve Outcomes*. Neuropharmacology, 2016.
- 423 11. Kreuter, J., *Nanoparticulate systems for brain delivery of drugs*. Advanced drug delivery
424 reviews, 2001. **47**(1): p. 65-81.
- 425 12. Al-Jamal, W.T. and K. Kostarelos, *Liposomes: from a clinically established drug delivery*
426 *system to a nanoparticle platform for theranostic nanomedicine*. Accounts of chemical
427 research, 2011. **44**(10): p. 1094-1104.
- 428 13. Chen, H.-P., et al., *A novel micelle-forming material used for preparing a theranostic vehicle*
429 *exhibiting enhanced in vivo therapeutic efficacy*. Journal of medicinal chemistry, 2015. **58**(9):
430 p. 3704-3719.
- 431 14. Luong, D., et al., *Polyvalent Folate-Dendrimer-Coated Iron Oxide Theranostic Nanoparticles*
432 *for Simultaneous Magnetic Resonance Imaging and Precise Cancer Cell Targeting*.
433 Biomacromolecules, 2017.
- 434 15. Luchetti, A., et al., *Monoclonal antibodies conjugated with superparamagnetic iron oxide*
435 *particles allow magnetic resonance imaging detection of lymphocytes in the mouse brain*.
436 Molecular imaging, 2012. **11**(2): p. 7290.2011. 00032.
- 437 16. Ramos-Cabrer, P. and F. Campos, *Liposomes and nanotechnology in drug development: focus*
438 *on neurological targets*. Int J Nanomedicine, 2013. **8**: p. 951-960.
- 439 17. Adibhatla, R.M., J. Hatcher, and K. Tureyen, *CDP-choline liposomes provide significant*
440 *reduction in infarction over free CDP-choline in stroke*. Brain research, 2005. **1058**(1): p. 193-
441 197.
- 442 18. Ramos-Cabrer, P., et al., *Serial MRI study of the enhanced therapeutic effects of liposome-*
443 *encapsulated citicoline in cerebral ischemia*. International journal of pharmaceutics, 2011.
444 **405**(1): p. 228-233.
- 445 19. Strehl, C., et al., *Effects of PVA-coated nanoparticles on human T helper cell activity*.
446 Toxicology letters, 2016. **245**: p. 52-58.

- 447 20. Imamura, S., et al., *The blood–brain barrier permeability of geissoschizine methyl ether in*
448 *Uncaria hook, a galenical constituent of the traditional Japanese medicine yokukansan.*
449 Cellular and molecular neurobiology, 2011. **31**(5): p. 787-793.
- 450 21. Chastellain, M., et al., *Superparamagnetic Silica-Iron Oxide Nanocomposites for Application*
451 *in Hyperthermia.* Advanced Engineering Materials, 2004. **6**(4): p. 235-241.
- 452 22. Kronberg, B., et al., *Preparation and evaluation of sterically stabilized liposomes: colloidal*
453 *stability, serum stability, macrophage uptake, and toxicity.* Journal of pharmaceutical
454 sciences, 1990. **79**(8): p. 667-671.
- 455 23. Wagner, S., et al., *Uptake mechanism of ApoE-modified nanoparticles on brain capillary*
456 *endothelial cells as a blood-brain barrier model.* PloS one, 2012. **7**(3): p. e32568.
- 457 24. Kayal, S. and R. Ramanujan, *Doxorubicin loaded PVA coated iron oxide nanoparticles for*
458 *targeted drug delivery.* Materials Science and Engineering: C, 2010. **30**(3): p. 484-490.
- 459 25. Rho, W.-Y., et al., *Facile synthesis of monodispersed silica-coated magnetic nanoparticles.*
460 Journal of Industrial and Engineering Chemistry, 2014. **20**(5): p. 2646-2649.
- 461 26. Wu, W., et al., *Recent progress on magnetic iron oxide nanoparticles: synthesis, surface*
462 *functional strategies and biomedical applications.* Science and technology of advanced
463 materials, 2015. **16**(2): p. 023501.
- 464 27. Deans, J.P., H. Li, and M.J. Polyak, *CD20-mediated apoptosis: signalling through lipid rafts.*
465 Immunology, 2002. **107**(2): p. 176-182.
- 466 28. Taylor, R.P. and M.A. Lindorfer, *Analyses of CD20 Monoclonal Antibody–Mediated Tumor*
467 *Cell Killing Mechanisms: Rational Design of Dosing Strategies.* Molecular pharmacology,
468 2014. **86**(5): p. 485-491.
- 469 29. Farrell, B.T., et al., *Using iron oxide nanoparticles to diagnose CNS inflammatory diseases and*
470 *PCNSL.* Neurology, 2013. **81**(3): p. 256-263.

471

Fig. 1.

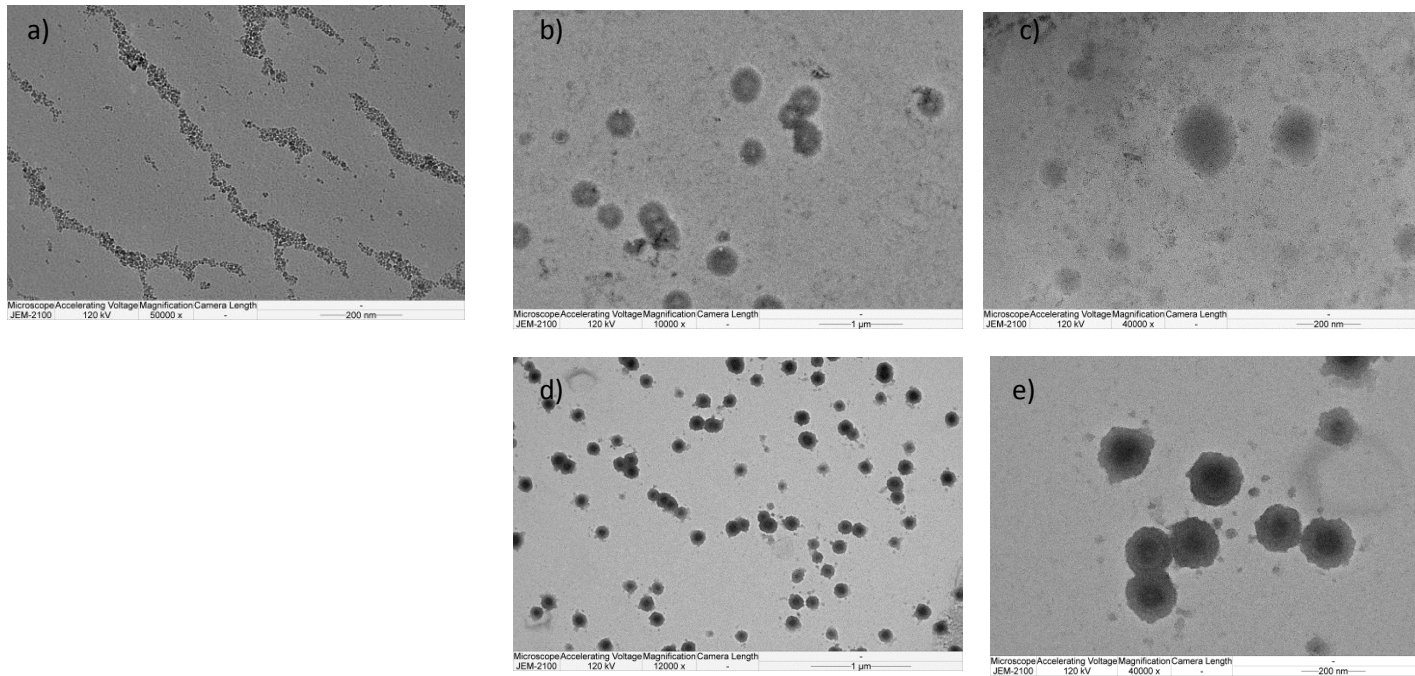


Figure 3. Morphology of liposome was magnified by Transmission Election Microscopy. a) SPIONs-PVA, b) and c) = bare liposome, d) and e) = SPIONs-PVA loaded liposome at 12,000 and 40,000 magnification, respectively.

Table 1 Physicochemical characterization of liposomes

Formulation	%w/w	Size (nm)		PDI		Zeta potential (mV)		% EE of SPIONs-PVA
		w/o SPIONs-PVA	w/t SPIONs-PVA	w/o SPIONs-PVA	w/t SPIONs-PVA	w/o SPIONs-PVA	w/t SPIONs-PVA	
Lip (liposome)	100	141.9 ± 1.0	129.9 ± 5.6	0.1 ± 0.1	0.3 ± 0.0	-0.1 ± 0.0	-2.3 ± 0.1	30.0 ± 4.1
Lip/PEG	90:10	169.7 ± 11.3	140.5 ± 16.2	0.1 ± 0.0	0.3 ± 0.0	-2.3 ± 0.3	-5.1 ± 0.7	27.3 ± 3.3
Lip/Tween80	90:10	161.0 ± 12.6	123.8 ± 19.5	0.2 ± 0.1	0.3 ± 0.1	-0.3 ± 0.0	-2.7 ± 0.4	41.4 ± 0.0
Lip/PEG/ Tween80	80:10:10	157.2 ± 9.1	136.4 ± 4.1	0.2 ± 0.0	0.2 ± 0.0	-2.2 ± 0.2	-5.6 ± 0.7	45.6 ± 8.2
Lip/PEG/ Tween80/Rituximab	79:10:10:1	182.0 ± 6.3	158.2 ± 13.3	0.2 ± 0.0	0.3 ± 0.0	-7.2 ± 0.4	-9.0 ± 0.1	44.6 ± 3.4

Fig. 2. MTT assay of liposome and SPIONs-PVA –loaded liposome

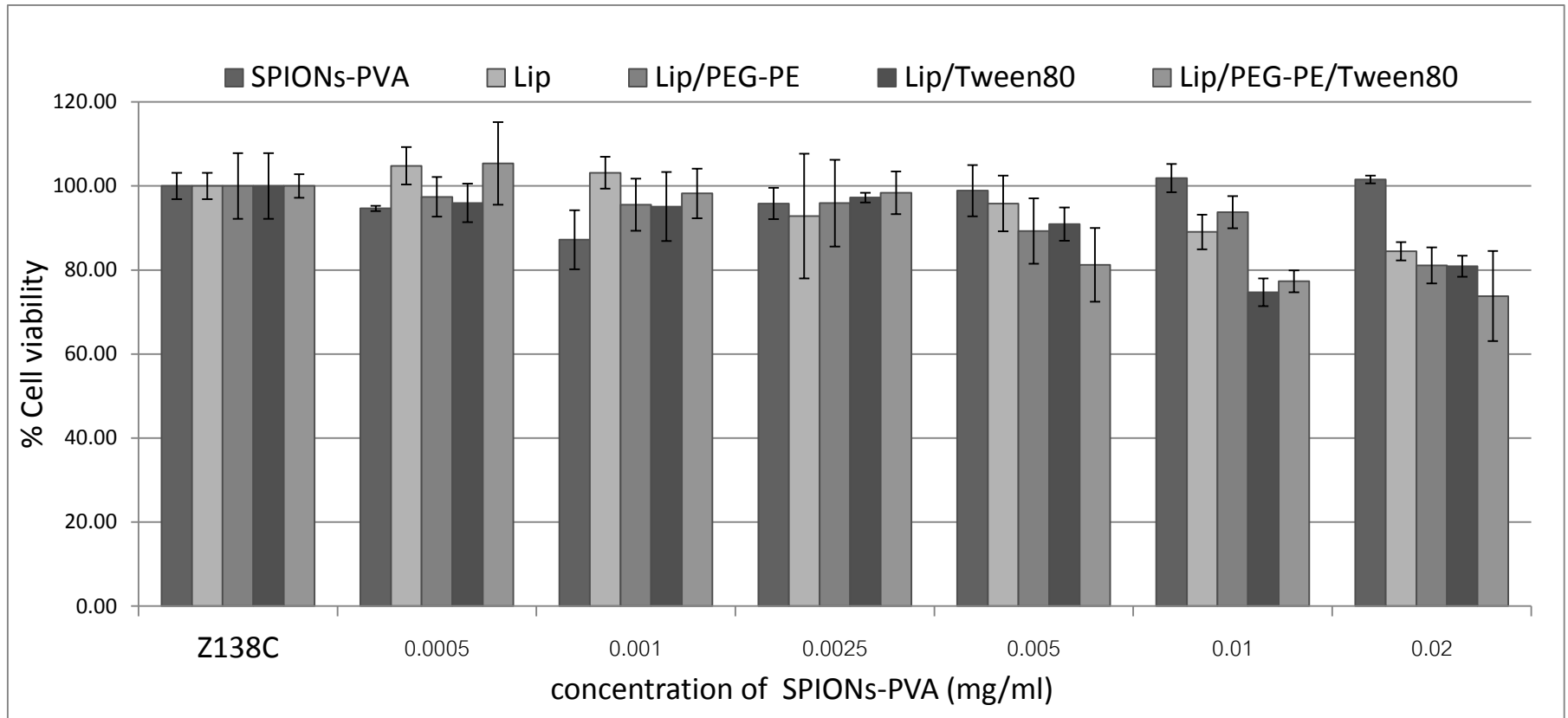
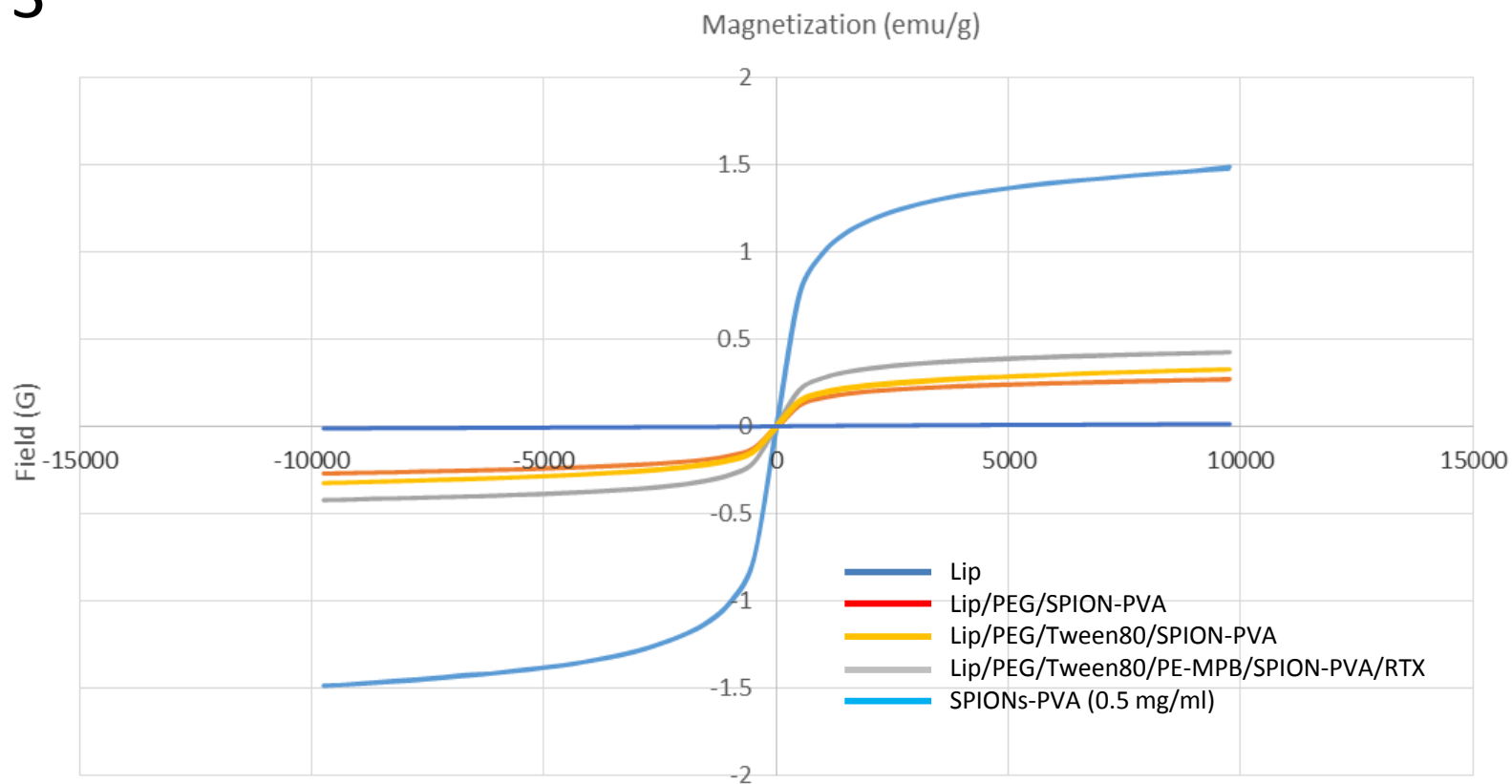


Table 2 stability of liposomes

Storage period	Lip		Lip/PEG/Tween80/SPIONs-PVA		Lip/PEG/Tween80/SPIONs-PVA/Rituximab	
	4 °C	25 °C	4 °C	25 °C	4 °C	25 °C
Size (nm)						
1 m	123.5 ± 10.1	156.8 ± 2.7	182.4 ± 16.3	167.9 ± 24.5	152.5 ± 30.0	159.2 ± 14.7
3 m	254.6 ± 8.1	227.1 ± 1.2	168.1 ± 7.9	244.7 ± 6.9	229.4 ± 5.5	285.7 ± 12.7
4 m	313.0 ± 16.9	379.7 ± 6.5	215.0 ± 19.5	242.0 ± 1.4	233.3 ± 8.0	236.4 ± 5.5
ζ(mV)						
1 m	-3.6 ± 0.0	-2.6 ± 0.2	-2.1 ± 0.4	-2.9 ± 0.2	-2.6 ± 0.0	-2.1 ± 0.0
3 m	-1.6 ± 0.2	-2.6 ± 0.0	-1.4 ± 0.0	-2.1 ± 0.0	-1.5 ± 0.1	-2.0 ± 0.1
4 m	-5.6 ± 0.7	-32.6 ± 0.1	-5.6 ± 0.4	-28.6 ± 0.7	-8.1 ± 2.0	-27.1 ± 1.1
PDI						
1 m	0.2 ± 0.0	0.2 ± 0.0	0.3 ± 0.0	0.3 ± 0.0	0.4 ± 0.1	0.4 ± 0.0
3 m	0.2 ± 0.0	0.2 ± 0.0	0.3 ± 0.0	0.3 ± 0.0	0.3 ± 0.0	0.3 ± 0.0
4 m	0.4 ± 0.0	0.5 ± 0.2	0.3 ± 0.0	0.2 ± 0.0	0.3 ± 0.0	0.3 ± 0.0

Fig. 3

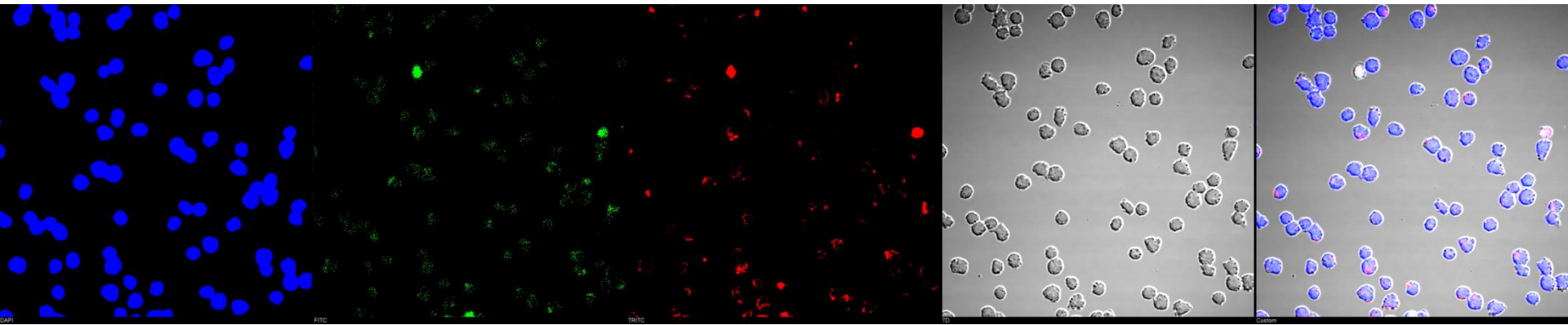


samples	Saturation magnetization (emu/g)
Lip	0.0
Lip/PEG/SPIONs-PVA	0.3
Lip/PEG/Tween80/SPIONs-PVA	0.3
Lip/PEG/Tween80/SPIONs-PVA/Rituximab	0.4
SPIONs-PVA (0.5 mg/ml)	1.5
Naked SPIONs	28.9

Fig. 4a

Z138C

Lip/PEG/Tween80/SPIONs-PVA



Lip/PEG/Tween80/SPIONs-PVA/Rituximab

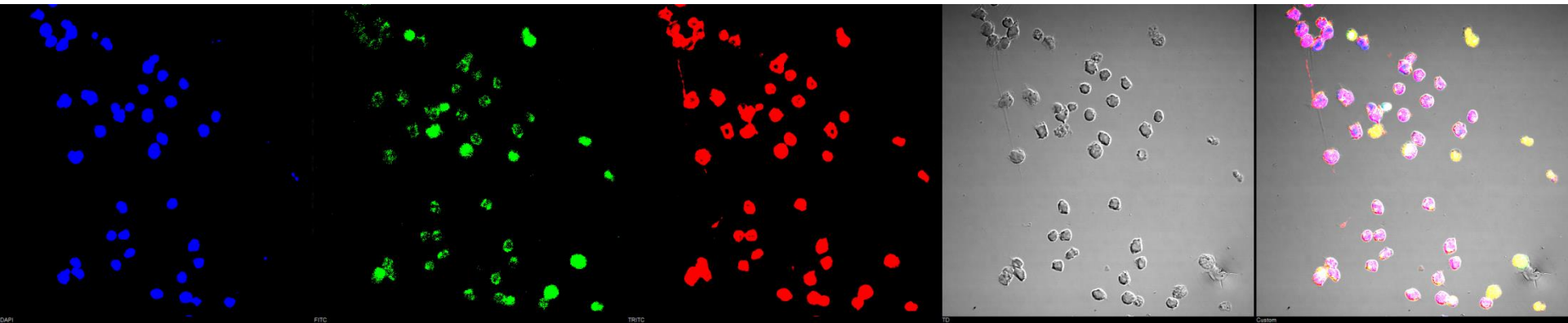
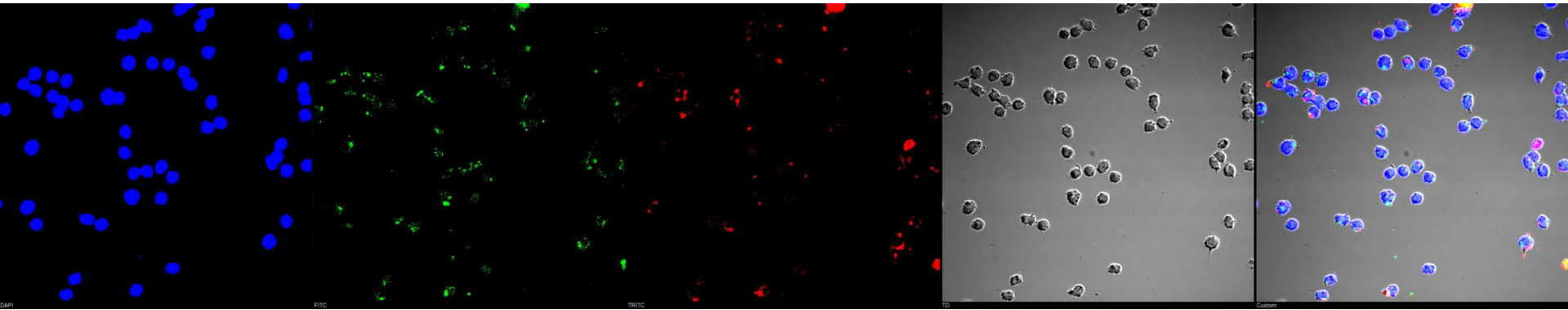


Fig. 4b

Granta

Lip/PEG/Tween80/SPIONs-PVA



Lip/PEG/Tween80/SPIONs-PVA/Rituximab

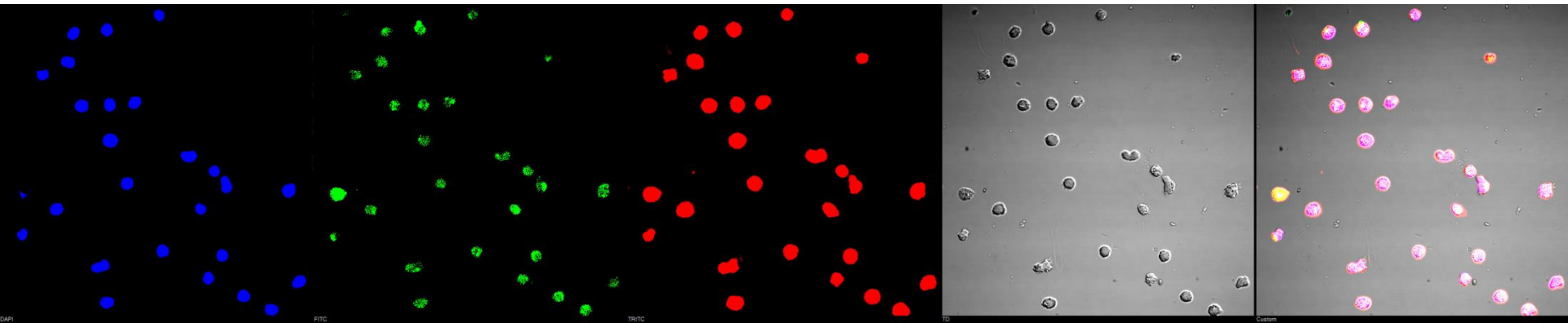
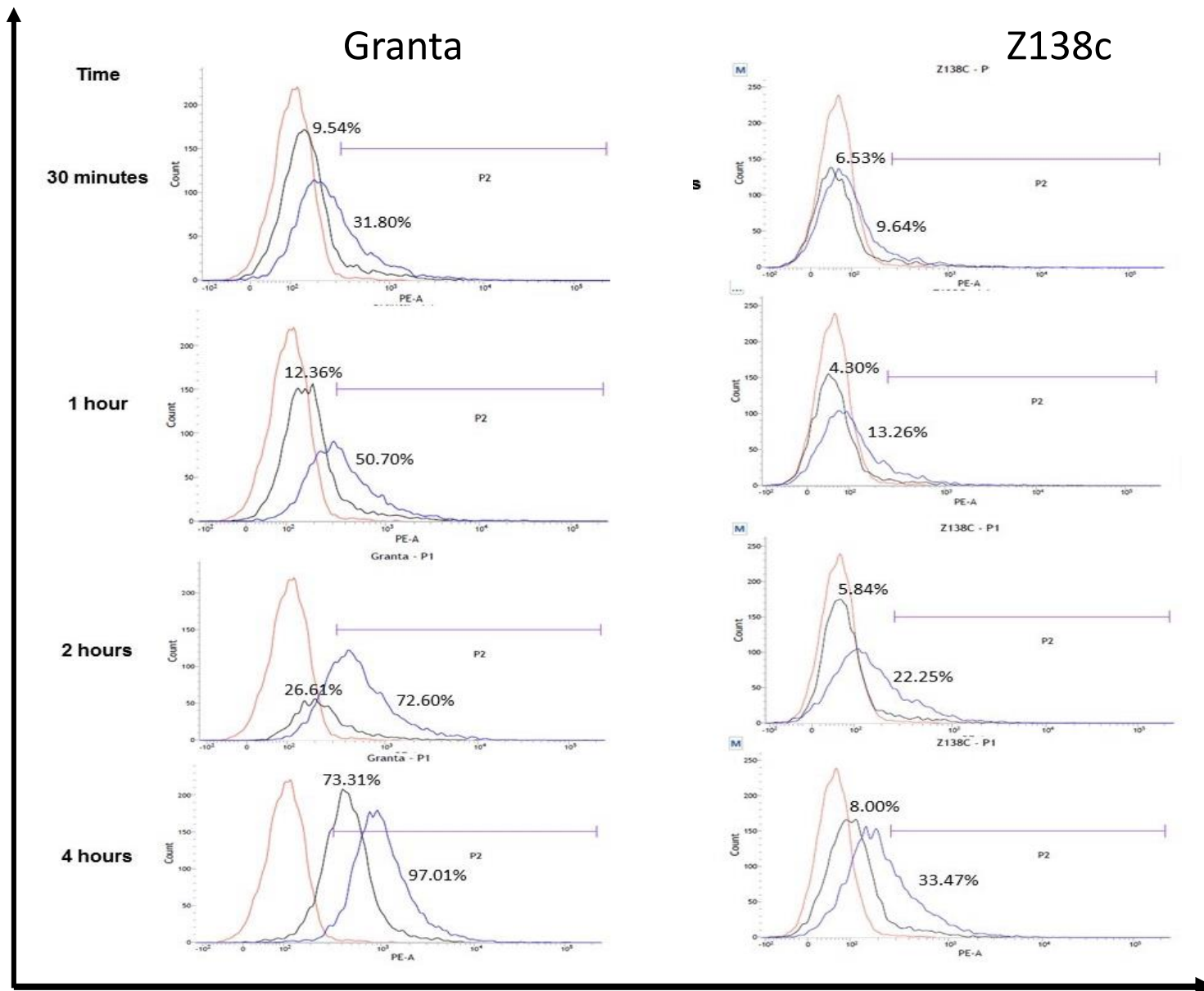


Fig. 5

counts



Red: cell control

Black: cell + Lip/PEG/Tween80/SPIONs-PVA

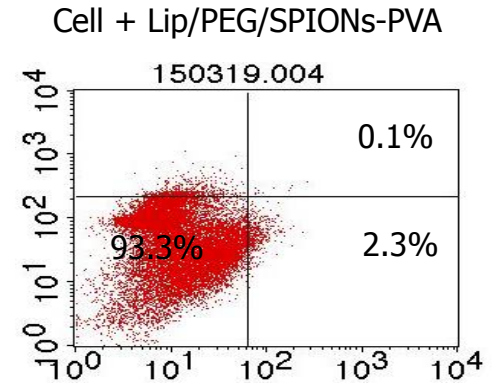
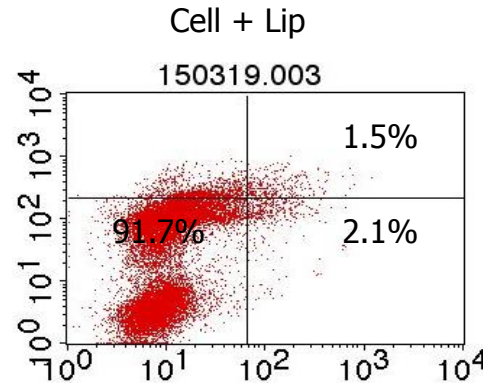
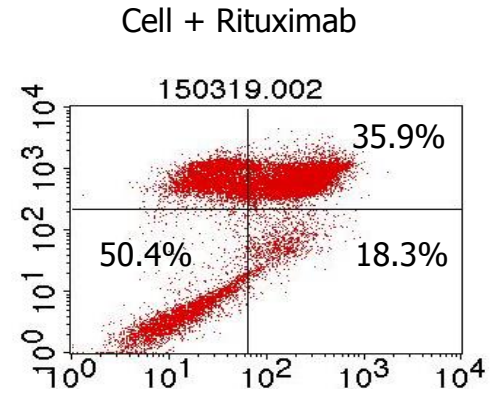
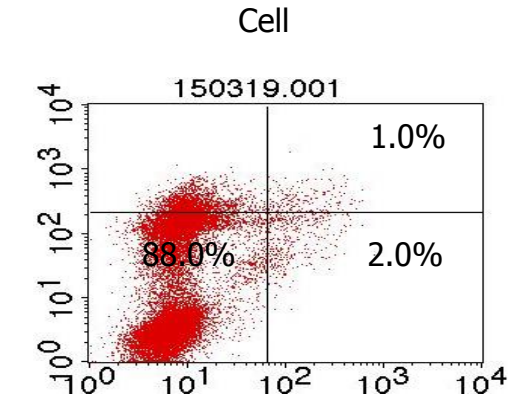
Blue: cell + Lip/PEG/Tween80/SPIONs-PVA/RTX

Dil dye

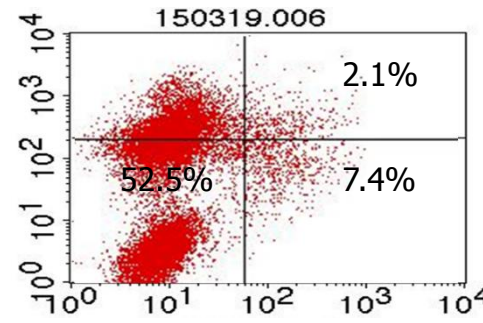
Fig. 6a

Granta

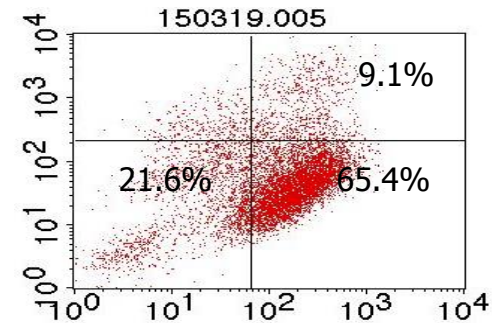
PI



Cell + Lip/PEG/Tween80/SPIONs-PVA



Cell + Lip/PEG/Tween80/SPIONs-PVA/Rituximab

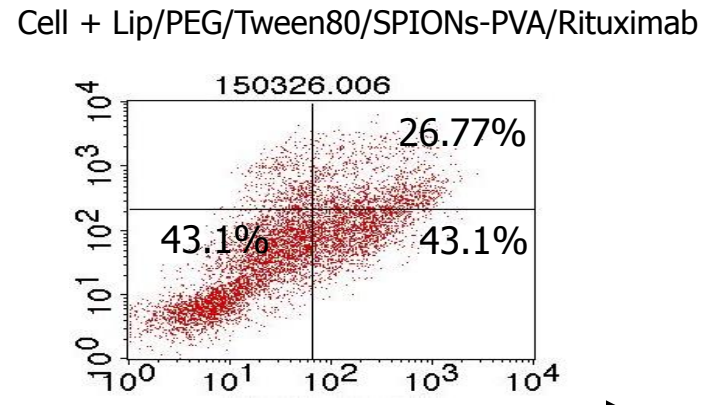
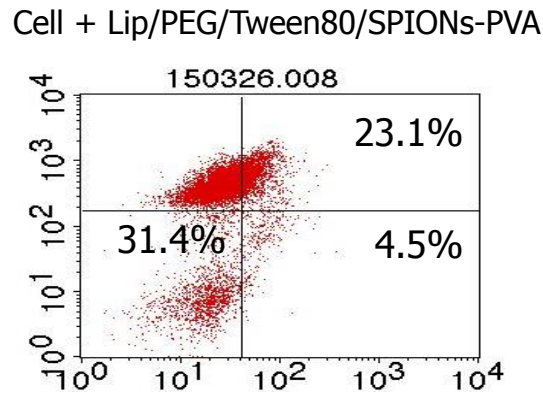
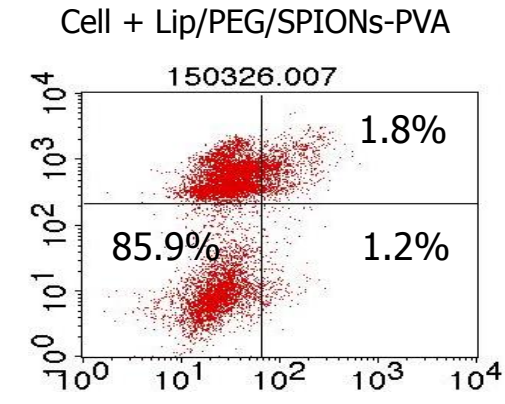
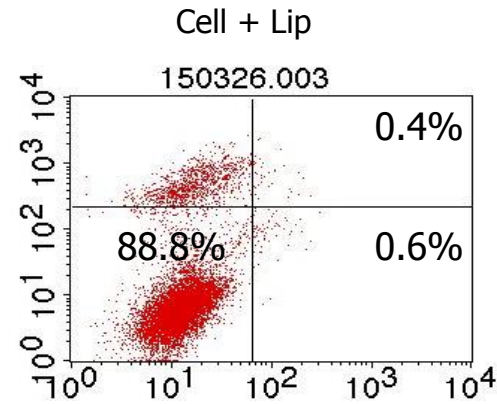
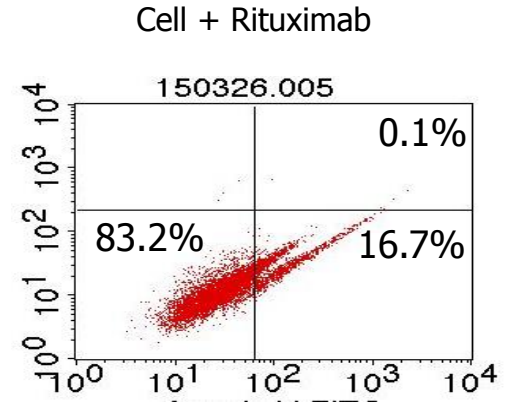
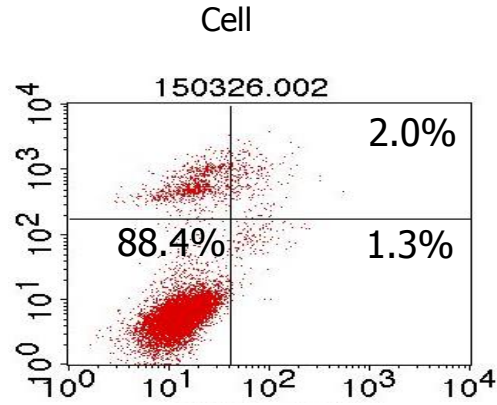


Annexin V-FITC

Fig. 6b

Z138c

PI



Annexin V-FITC

Fig. 7

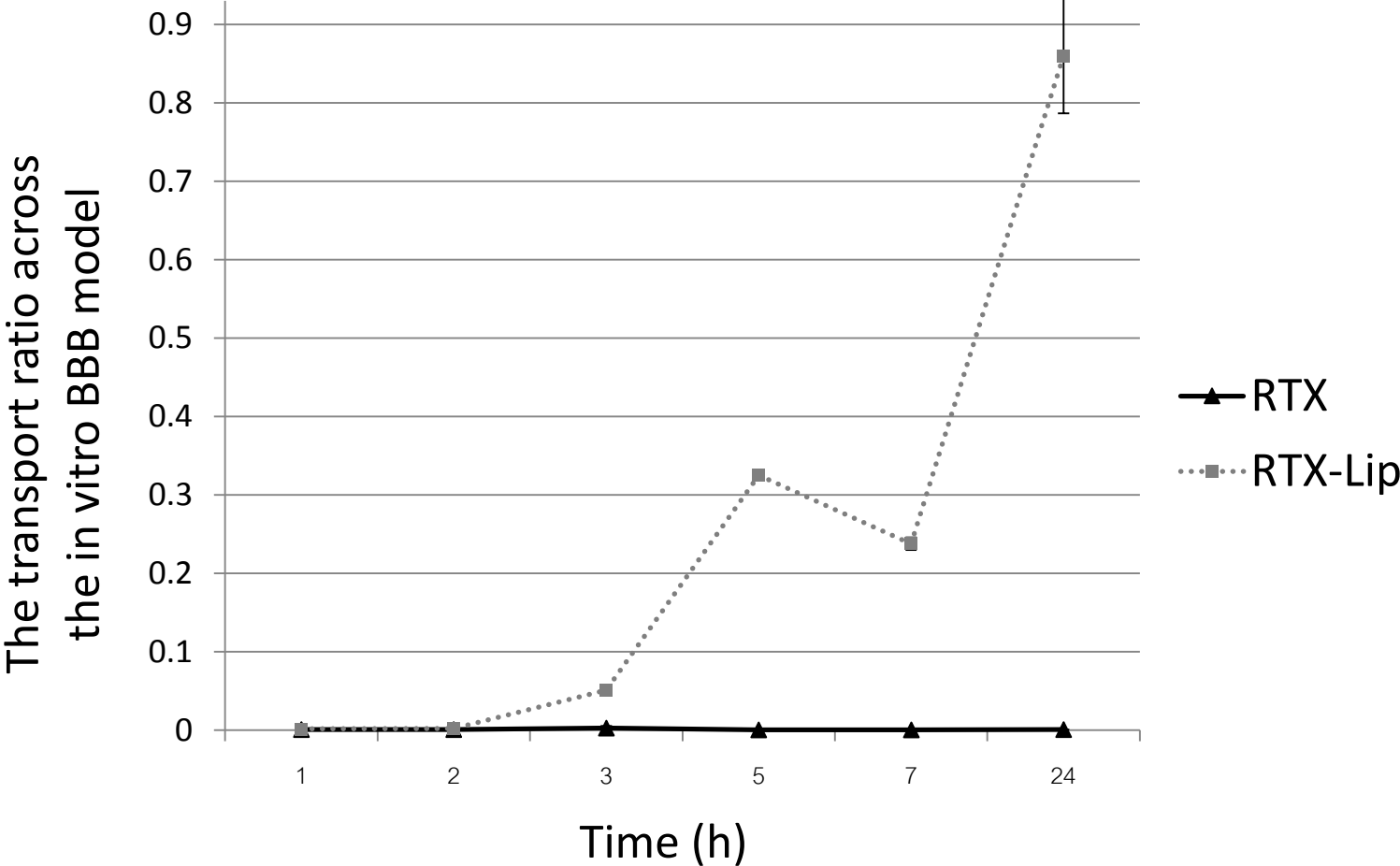


Fig. 8

Therapeutic effect

